

Article

Analysis of Outburst Coal Structure Characteristics in Sanjia Coal Mine Based on FTIR and XRD

Anjun Jiao ¹, Shixiang Tian ^{1,2,*} and Huaying Lin ¹ 

¹ College of Mining Engineering, Guizhou University, Guiyang 550025, China; jj182204759@gmail.com (A.J.); eternity37326@gmail.com (H.L.)

² The National Joint Engineering Laboratory for the Utilization of Dominant Mineral Resources in Karst Mountain Area, Guizhou University, Guiyang 550025, China

* Correspondence: husttsx@163.com

Abstract: In order to reveal the distribution characteristics of functional groups and the difference of microcrystalline structure parameters between outburst coal and primary coal, the coal samples inside and outside the outburst holes of the Sanjia coal mine were examined. The functional groups and microcrystalline structure parameters of outburst coal and primary coal in the Sanjia coal mine were studied by infrared spectroscopy, X-ray diffraction (XRD) experiment and peak-splitting fitting method. The results showed that the substitution mode of the benzene ring in an aromatic structure was mainly benzene ring tri-substituted, with primary coal of 32.71% and outburst coal of 31.6%. The primary coal contained more functional groups, from which hydrogen bonds can easily be formed, meaning that gas is not easily adsorbed by coal. The aromatic hydrogen rate (f_{Ha}) of the outburst coal was 0.271, the aromatic carbon rate (f_c) was 0.986, the aromaticity I_1 was 0.477, I_2 was 0.373 and the length of the aliphatic branched chain (A_{CH_2}/A_{CH_3}) was 0.850. Compared with the primary coal, the aromatic hydrogen rate, aromatic carbon rate and the aromaticity of the outburst coal were higher, indicating that the hydrogen and carbon elements in the aromatic functional groups of outburst coal were higher and that the aliphatic functional group was higher than the aromatic structural functional group. A_{CH_2}/A_{CH_3} and maturity (Csd) were slightly lower than those of primary coal, indicating that the coal has more straight chains than side chains, while aliphatic hydrocarbons are mostly short chains and have high branched degree. There were obvious 002 and 100 peaks in the XRD pattern. The d_{002} and d_{100} of outburst coal were 3.570 and 2.114, respectively, while the number of effective stacking aromatics was 3.089, which was lower than that of primary coal, indicating that the structure of the dense ring in the coal saw certain changes.

Keywords: outburst coal; primary coal; structural parameters; infrared spectrum; XRD



Citation: Jiao, A.; Tian, S.; Lin, H. Analysis of Outburst Coal Structure Characteristics in Sanjia Coal Mine Based on FTIR and XRD. *Energies* **2022**, *15*, 1956. <https://doi.org/10.3390/en15061956>

Academic Editor: Nikolaos Koukoulas

Received: 30 January 2022

Accepted: 3 March 2022

Published: 8 March 2022

Publisher's Note: MDPI stays neutral with regard to jurisdictional claims in published maps and institutional affiliations.



Copyright: © 2022 by the authors. Licensee MDPI, Basel, Switzerland. This article is an open access article distributed under the terms and conditions of the Creative Commons Attribution (CC BY) license (<https://creativecommons.org/licenses/by/4.0/>).

1. Introduction

Guizhou Province in south China has abundant coal resources, wide distribution and complete coal types; however, the natural occurrence conditions of coal seams in Guizhou are poor, the occurrence of gas is complex and its control is difficult at underground mines [1–3]. In its natural state, gas exists in coal or surrounding rock in a free state and suction state [4–8]. The functional group of coal determines the chemical adsorption characteristics of coal, which is mainly controlled by the maceral and mineralogical compositions of coal seams and could indirectly affect the adsorption state of gas by coal seams [9–18]. Therefore, it is of great significance to study the functional group distribution and microcrystalline structure parameters of coal in order to understand gas occurrence and predict gas disasters.

Due to the complex microstructure characteristics of coal, our understanding of coal chemical composition is still limited and under discussion. For a long time, the research on the chemical structure of coal and the characteristics of functional groups in coal has

been the mainly focus of several studies [19–23]. Infrared spectroscopy is a non-destructive structural characterization technique that is especially suitable for qualitative and semi-quantitative study of functional groups in coal [24–28]. It is very suitable for characterizing insoluble organic compounds in coal. It is the comprehensive absorbance estimation of organic components based on the main functional groups (such as alkyl CH, CH₂ and CH₃, aromatic C=C and C-H, carbonyl/carboxylic acid C=O, hydroxyl-OH) [29,30]. Based on this, several studies have been conducted during the last two decades. Ibarra et al. [31] assigned the absorption peak of the whole spectrum and divided the whole spectrum into four parts, namely, aromatic structure, oxygen-containing functional group, fatty functional group and hydroxyl functional group. Sobkowiak et al. [32] studied the distribution characteristics of aromatic and aliphatic functional groups in coal by infrared spectroscopy. Rosa et al. [33] and Alemany et al. [34], who focused on the characterization of Illinois No.6 coal samples, found that the aromaticity of the coal was 0.72, 0.7 and 0.68. Painter et al. [35] summarized the assignment of hydroxyl absorption peaks in infrared spectroscopy coal, finding that hydroxyl hydrogen bonds are mainly OH- π , OH-OH, OH-ether oxygen. Orrego-Ruiz et al. [36] used FTIR spectroscopy to determine five Colombian coals and obtained the contents of aliphatic hydrogen and aromatic hydrogen. Cao et al. [37] found that the substitution degree of high maturity coal decreases rapidly in the early stage of coalification. There are a large number of aromatic clusters in semi anthracite and anthracite, and the average aromatic ring size is above 3–4.

X-ray diffraction (XRD) is an important technique for determining the structural parameters of crystalline matter in coal, which is also widely used in studying the polynuclear aromatic structure and the composition of microcrystal aromatic ring lamellae of amorphous materials [38–42]. Saikia et al.'s [43] XRD and FTIR analysis of the coal samples from Makum and Assam states in India indicated that the intensities of carbonyl groups content in coal was related to the metamorphic degree of coal. Wu et al. [44] found that there was an exponential relationship between XRD structure parameters and C/H by analyzing the XRD spectra of nine coals. Jiang et al. [45], according to the XRD pattern of medium and high rank coal, concluded that there is a linear relationship between XRD structural parameters and vitrinite reflectance (%R_o). Boral P et al. [46] studied five coal samples selected from different coal pools in India using X-ray diffraction. It was found that d_{002} and f_a values depend on coal rank, not only carbon content.

Even though the previous studies mainly focused on the functional groups and microstructure of primary coal and tectonic zone coal, the research on functional groups and the microstructure of coal samples in outburst sites is limited, and the above research is less related to the research and analysis of outburst coal in the Guizhou mining area. In order to explore the distribution of functional groups in outburst coal and the characteristics of microcrystalline structure parameters, this paper intends to use an infrared spectroscopy test and peak fitting method to study the infrared spectrum of coal samples and determine the structural parameters of its coal samples. Secondly, the microcrystalline structure parameters of coal samples were calculated by XRD analysis. Finally, the functional groups and microcrystalline structure parameters of outburst coal samples and primary structure coal samples were compared, and the differences between the two were analyzed to better explain the influence of outburst coal on gas occurrence.

2. Sample Preparation and Test Method

2.1. Sampling Cite

The Sanjia coal mine is located in the south-west section of the Guiyang complex tectonic deformation zone of Tailong in the north of the Yangtze platform in the south-east wing of Guanzhai syncline. In general, it is a monoclinic structure, with strata moving towards the northeast, tending to the northwest, and with inclination of about 10°. The faults found in the mining area are located in the southern part of the mining area and its edge. Affected by the faults, the strata have changed. On 25 November 2019, a prominent accident occurred at the heading face of the 41,601 transport roadway in Sipan District. The

sampling point selected in the 41,601 transport roadway heading face was located near the northern boundary of the mining area. See Figure 1.

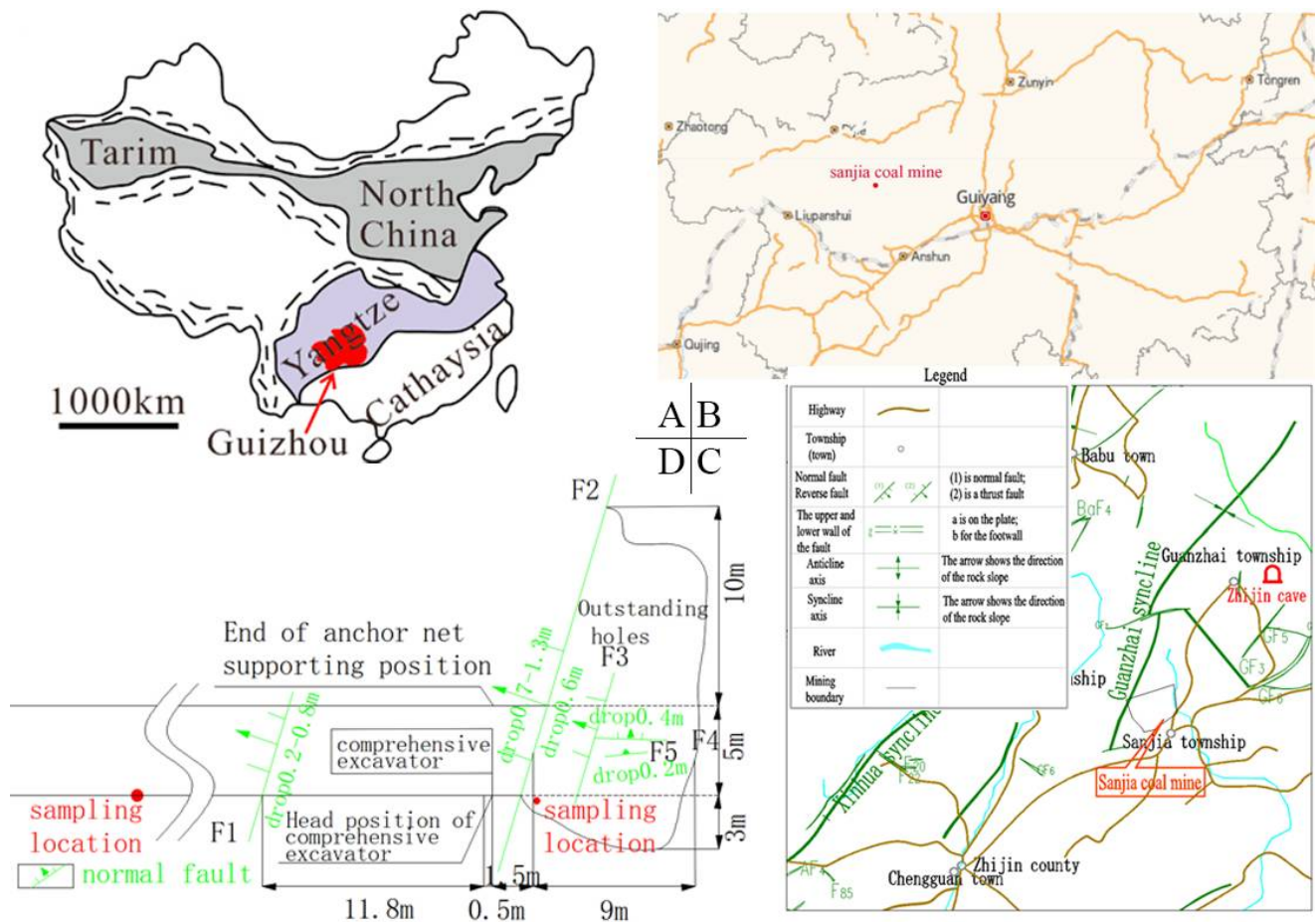


Figure 1. Prominent position diagram. Note: (A,B) are the geographical location of the mine; (C) is the geological structure near the mine; (D) is a prominent geological structure.

2.2. Proximate and Ultimate Analyses of Coal Samples

Samples were gathered soon after the outburst accident. The surface oxide layer of the sampling point was stripped and the outburst coal samples were taken in the outburst hole by the groove method, while the primary coal samples were taken outside the outburst hole. The collected coal samples were immediately sealed in the coal sample tank to reduce exposure to the external environment, the oxidation of the samples were slowed down during the period before the start of the experiment, and the sampling point information was recorded. The tank was fixed in the transport process to prevent secondary damage to coal. The samples were sent to the laboratory and ground into the specified particle size by agate bowl. According to GB/T 214-2007 and SN/T 4764-2017, coal ash, moisture, volatile content and C, H, N, O, S and other elements were determined by industrial analyzer and elemental analyzer.

2.2.1. Infrared Spectroscopy Experiments

The experiment was carried out by Nicolet 6700 Fourier transform infrared spectrometer. Before the experiment, the coal samples were placed in a constant temperature oven at 80 °C for 5 h for drying treatment. After drying, the coal samples were fully mixed with potassium bromide (KBr) at a ratio of 1:100, and then loaded into the grinding tool to make transparent sheets of 0.1–1 mm thickness on the tablet press. The equipment test conditions

were: a wave number test range of 7800–375 cm^{-1} , a scanning rate of 0.158–6.33 cm/s , an infrared spectral resolution of 4 cm^{-1} and scanning times of 32.

2.2.2. X-ray Diffraction (XRD) Analysis

The X-ray diffractometer used the X-ray with a fixed wavelength to irradiate the coal. When the wavelength of the X-ray was consistent with the magnitude of the lattice in the coal, the diffraction phenomenon occurred. Different diffraction light was formed at different positions. A series of X-rays irradiated at different angles were recorded to form. According to the map, the data provided about the crystalline structure of the coal was analyzed [47]. In the experiment, the X-ray diffractometer Shimadzu XRD-6100 was used for analysis and testing, and the coal samples that had been prepared in advance were loaded onto the support. Setting working conditions, the light source was an X-ray tube copper that targeted radiation ($\gamma = 0.15405 \text{ nm}$) and that had a voltage of 40 kV, a current of 40 mA, a scanning speed of 10/mm and a scanning range of 0–90°.

3. Experimental Results and Analysis

3.1. Standard Coal Quality Parameters

It can be seen from the composition analysis of the coal samples that the outburst coal has higher volatile matter and ash content than the primary coal and that the moisture content of the primary coal is higher than that of the outburst coal. Except hydrogen, the elements of outburst coal are higher than that of the primary coal. The test results are shown in Table 1.

Table 1. Coal sample analysis table.

Component Coal Samples	Proximate Analysis			Ultimate Analysis				
	$A_{ad}/\%$	$V_{ad}/\%$	$M_{ad}/\%$	C	H	N	S	O
outburst coal	6.1	5.4	4.6	82.9	2.87	1.51	0.42	4.05
primary coal	9.3	4.7	4.3	81.7	2.69	1.65	0.38	3.92

Note: M_{ad} = moisture content (wt%, dry basis), A_{ad} = ash (wt%, dry basis), V_{ad} = volatile (wt%, dry basis), FC_{ad} = fixed carbon (wt%, dry basis).

3.2. FTIR Fitting Spectral Characteristics Analysis

The infrared spectra of raw coal and outburst coal samples were obtained by an infrared spectrum test of coal samples, as shown in Figure 2 and Table 2. In the process of the infrared spectrum test, due to the complex composition of coal, the absorption bands of many functional groups in coal provided the infrared spectrum. In addition, the wave number distribution range of the spectrum is wide, meaning that it is easy to cause spectral superposition and difficult to determine the position and intensity of absorption peaks. Through the peak fitting of the original spectrum of the coal samples, the parameters and attribution of absorption peaks are determined, and the change characteristics of infrared spectrum of coal samples are thus more truly reflected. The infrared spectrum of coal samples can be divided into four absorption bands: aromatic structure absorption band, oxygen-containing functional group absorption band, fat structure absorption band and hydroxyl absorption band. The corresponding wave numbers are 700–900 cm^{-1} , 1000–1800 cm^{-1} , 2800–3000 cm^{-1} , 3000–3600 cm^{-1} , respectively, as shown in Figure 2.

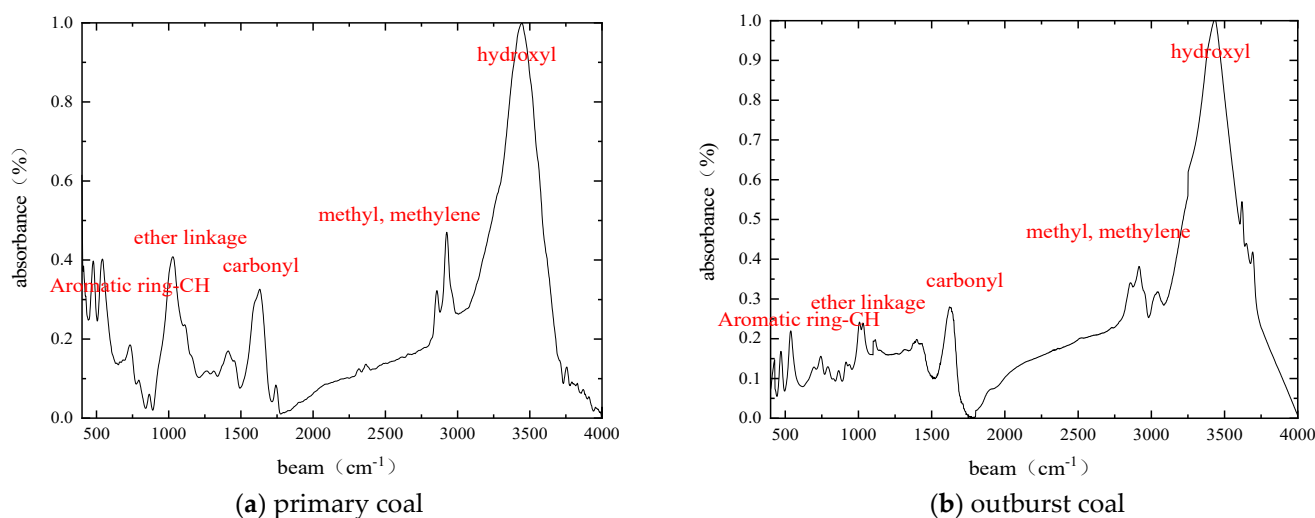


Figure 2. Fourier infrared spectra of coal samples.

Table 2. Ratios of various functional groups.

Coal Samples	Component	Functional Groups Ratios			
		AS/%	OC/%	FS/%	HY/%
outburst coal		2.19	16.10	7.38	43.34
primary coal		2.71	24.58	7.27	42.31

Note: AS = aromatic structure absorption band; OC = oxygen-containing functional group absorption band; FS = fat structure absorption band; HY = hydroxyl absorption band.

3.2.1. Absorption Band of Aromatic Structure

It can be seen from Figure 3 that the original spectra of aromatic structures in the two coals are different. There are three peaks in the primary structure coal and four peaks in the outburst coal. In order to make the fitted spectra closer to the experimental results, 11–14 peaks were fitted, and the correlation coefficients were more than 99.9%. The 700–900 cm^{-1} absorption band is the absorption vibration of the aromatic structure, which is an important characteristic peak for identifying the substitution mode of the aromatic rings in the coal. Among them, 730–750 cm^{-1} is the disubstituted absorption peak, 750–810 cm^{-1} is the trisubstituted absorption peak, 810–850 cm^{-1} is the tetrasubstituted absorption peak and 850–900 cm^{-1} is the pentasubstituted absorption peak.

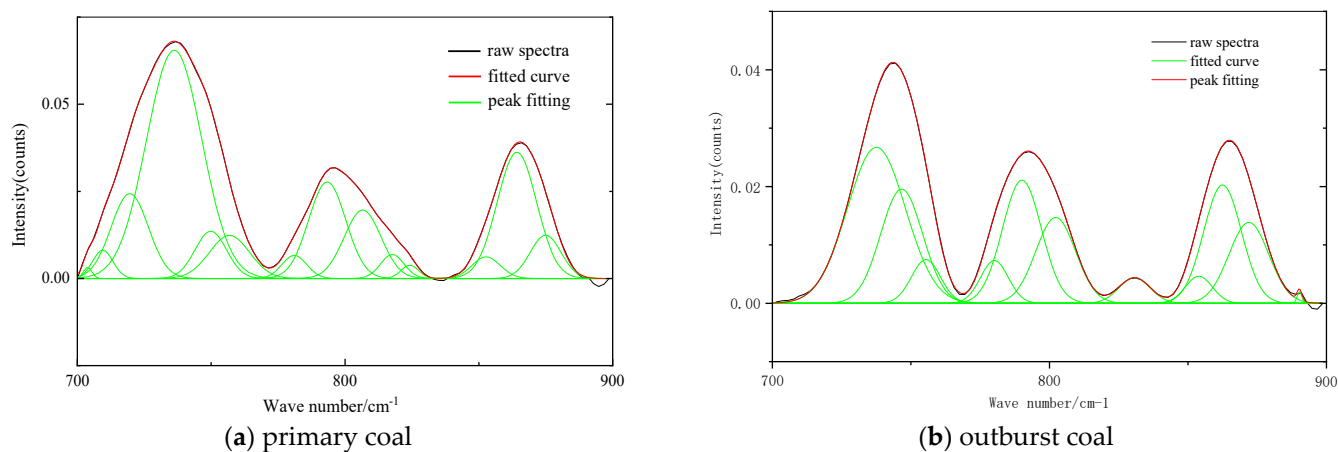


Figure 3. FTIR Spectra of Aromatic Structure.

According to the above four kinds of wave number classification statistics, the different benzene ring substitution column diagram was obtained (see Figure 4). The substitution of the benzene ring in the aromatic structure was mainly the trisubstituted benzene ring, and the proportion of primary structure coal reached 32.71%. With the increase of heating impact, the outburst coal decreased to 31.6%, and the difference was small. The disubstituted benzene ring decreased from 19.56% to 12.98%, the tetrasubstituted benzene ring increased from 8.93% to 16.89% and the pentasubstituted benzene ring increased from 10.91% to 22.10%. Among them, the values of the tetrasubstituted benzene ring and the pentasubstituted benzene ring are 1.89 times and 2.02 times of primary coal, respectively. The factors that cause this phenomenon are diverse, but may include the substitution reaction of the cyclization of the aliphatic chain and the positioning group on the aromatic ring.

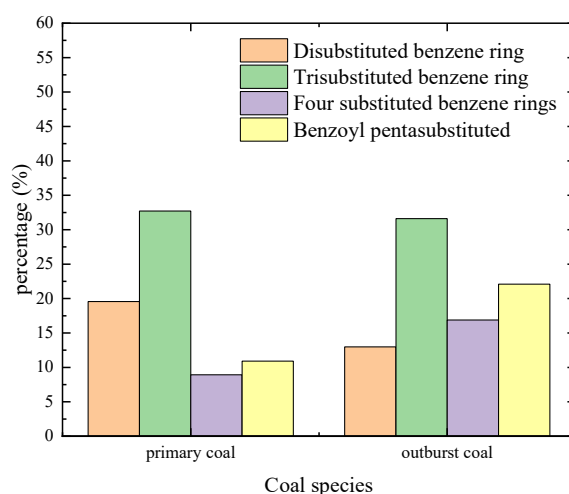


Figure 4. Statistical distribution of substituted benzene rings.

3.2.2. Absorption Band of Oxygen Functional Groups

It can be seen that the absorption band of $1000\text{--}1800\text{ cm}^{-1}$ is the stretching vibration of oxygen-containing functional groups, and the absorption peaks of $1000\text{--}1300\text{ cm}^{-1}$ are mainly attributable to the C-O stretching vibration of phenols, alcohols, ethers and esters (Figure 5). The peak positions at $1375\text{--}1460\text{ cm}^{-1}$ were symmetric and antisymmetric deformation vibrations of methyl, while the peak at $1800\text{--}1530\text{ cm}^{-1}$ had the stretching vibration of -COOH- and CO.

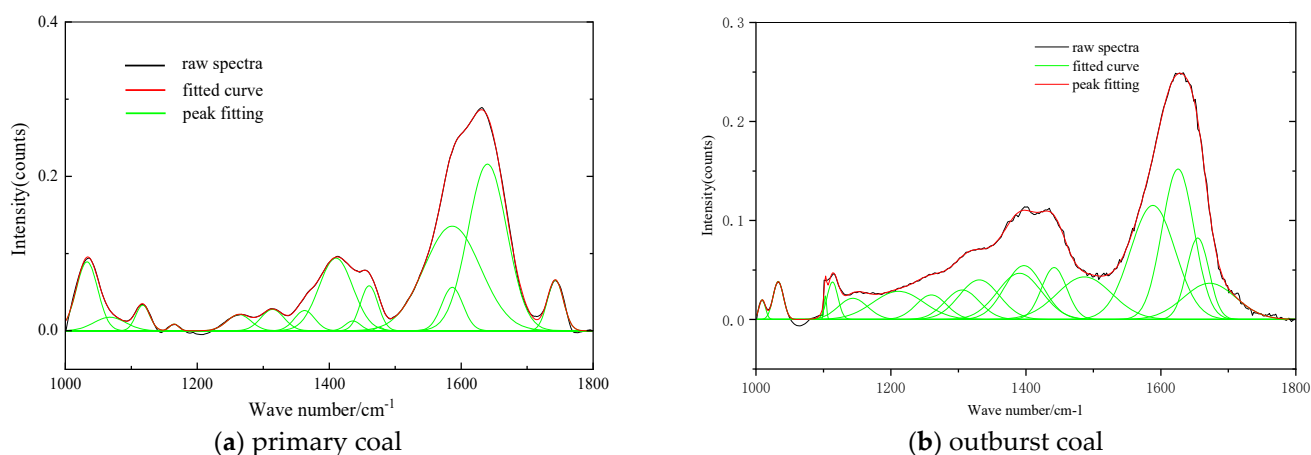


Figure 5. FTIR Spectra of Oxygen Functional Group Structure.

The percentage of C-O, C=O and C-C in these two coal samples were counted and the histogram was obtained, as shown in Figure 6. It can be concluded that with the increase of heating impact, the content of C-O increased from 14.97% of the primary structure coal to 19.86% of outburst coal, and the content of C-C increased from 17.33% of primary structure coal to 19.47% of outburst coal. Among them, the content of C=O changed most obviously, from 3.82% of primary structure coal to 6.84% of outburst coal, which increased by 44.15%, indicating that the content of carbon and oxygen elements in outburst coal was accumulated due to increased temperature during outburst.

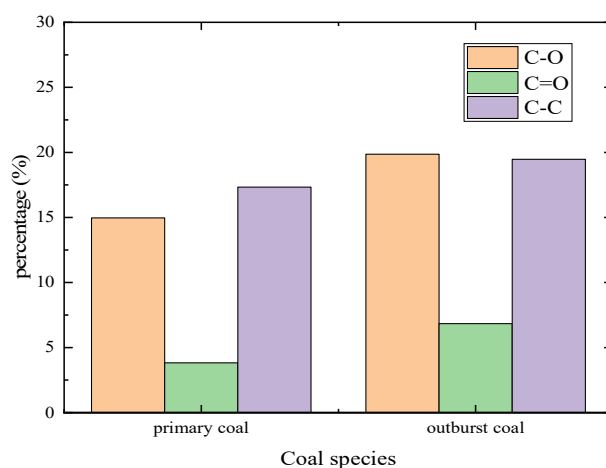


Figure 6. Statistical distribution histogram of oxygen-containing functional groups' structure content.

3.2.3. CHal Structure Absorption Band

It can be seen from Figure 7 that the absorption band of 2800–3000 cm^{-1} was the absorption vibration of CHal stretching structure. The spectrum was fitted with 6–7 peaks, and the fitting degree reached more than 99.9%. The coal contains methyl, methylene and methylene. The peak at 2853 cm^{-1} is the symmetric stretching vibration of methylene, the peak at 2871 cm^{-1} is the symmetric stretching vibration of methyl, the peak at 2895 cm^{-1} is the stretching vibration of methylene, the peak at 2923 cm^{-1} is the antisymmetric stretching vibration of methylene and the peak at 2953 cm^{-1} is the antisymmetric stretching vibration of methyl.

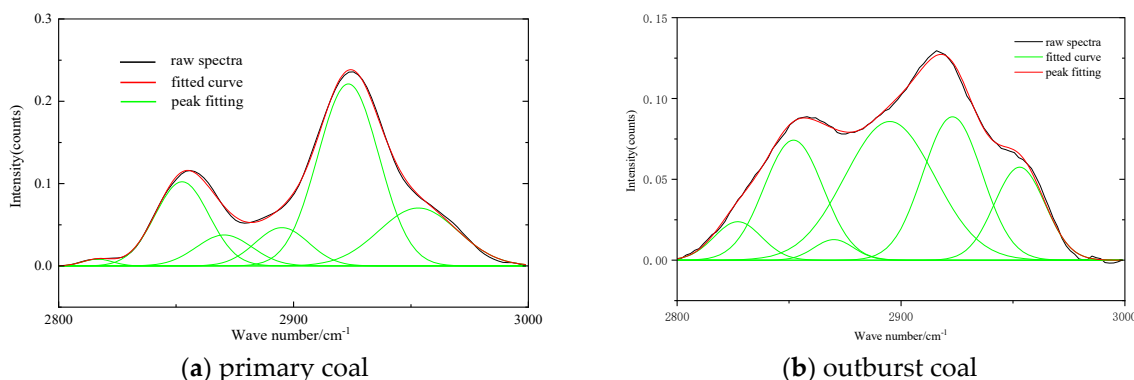


Figure 7. FTIR spectra of CHal structure.

The aliphatic bands in the studied coal samples were statistically analyzed to get the histogram (see Figure 8). The content of methylene symmetric stretching vibration in raw coal and outburst coal was 18.73% and 20.10%, respectively. The content of symmetric stretching vibration of methyl was 7.14% and 2.31%, respectively. Compared with the primary coal, the outburst coal had a significant downward trend, which was reduced by 67.65%. The content of methylene stretching vibration was 8.47% and 35.11%, respectively.

The stretching vibration of outburst coal methylene increased rapidly, and the change value increased 4.15 times. The content of antisymmetric stretching vibration of methylene was 45.95% and 24.02%, respectively. The content of antisymmetric stretching vibration of methyl was 18.87% and 13.33%, respectively. It may be that the thermal effect of the outburst process leads to the volatilization of hydrogen or the fracture of the fat chain.

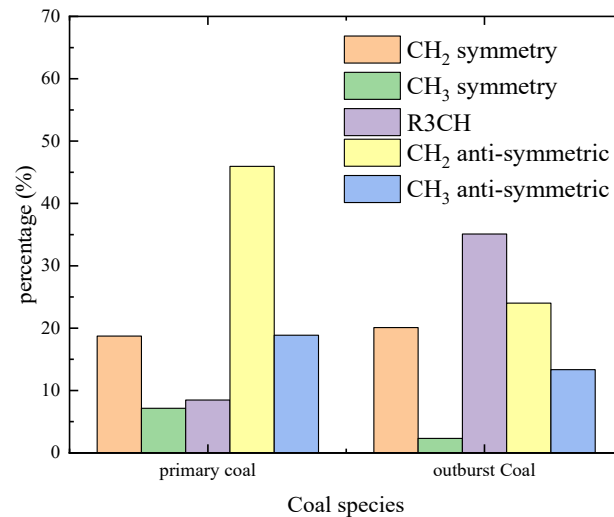


Figure 8. Statistical distribution histogram of CHal.

3.2.4. Hydroxyl Absorption Band

It can be seen from Figure 9 that the absorption band of 3000–3600 cm^{-1} was the absorption vibration of the hydroxyl structure. The spectrum was fitted with 4~5 peaks, and the fitting degree reached more than 99.9%, which was closer to the original spectrum. There are several O-H stretching vibration absorption peaks in 3200–3516 cm^{-1} , forming a wide and scattered absorption band. There is a sharp absorption peak at 3611 cm^{-1} , which is the absorption peak of free-OH.

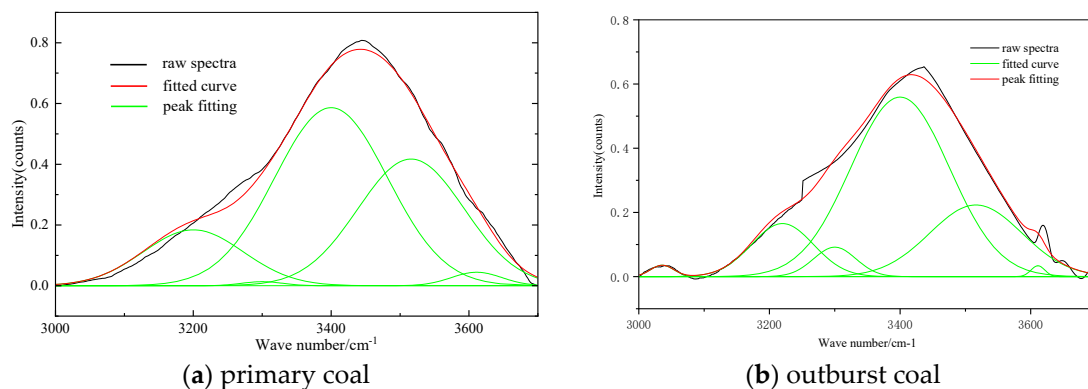


Figure 9. FTIR fitting spectra of hydroxyl structure.

The types of hydrogen bonds in the coal hydroxyl groups were analyzed, and the histogram was obtained, as shown in Figure 10. Hydrogen bonds exist in coal, and the content of cyclic associative hydrogen bonds in primary coal and outburst coal accounts for 13.97% and 11.24%, respectively. The content of self-associated hydroxyl accounted for 50.40% and 60.60%, respectively; the increase of self-association hydroxyl content is due to the tighter internal structure of the molecule, which increases the probability of self-association hydroxyl synthesis. When water molecules and methane compete on the surface of coal, water molecules are more likely to seize the adsorption site. Water

molecules' adsorption replaces gas adsorption and indirectly reduces gas adsorption in coal seams.

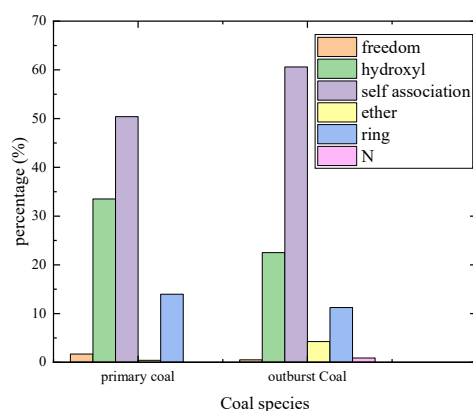


Figure 10. Column diagram of hydrogen bond type statistical distribution in hydroxyl group.

3.3. Analysis of FTIR Structural Parameters

In order to analyze the macromolecular structure of coal, the chemical structure parameters and significance of coal are generally quantitatively analyzed through structural parameters such as aromatic hydrogen rate, aromatic carbon rate, aromaticity, polycondensation degree of the aromatic ring, length of aliphatic chain, branching degree and the maturity of the coal.

3.3.1. Hydrogen Aromaticity f_{H_a}

Aromatic hydrogen rate [44] is the percentage of hydrogen atoms in aromatic compounds. It is assumed that only aromatic hydrogen and aliphatic hydrogen exist.

$$f_{H_a} = \frac{H_a}{H} \frac{A_{900\sim 700\text{cm}^{-1}}}{A_{900\sim 700\text{cm}^{-1}} + A_{3000\sim 2800\text{cm}^{-1}}} \quad (1)$$

where H_a is the number of H atoms of aromatic compounds. H is the number of H atoms.

3.3.2. Aromatic Carbon Ratio f_C

Aromatization rate indicates the proportion of carbon atoms in aromatic hydrocarbons. Calculation of aryl carbon ratio supposes only aryl carbon and lipocarbon exist in carbon atom.

$$f_C = 1 - \frac{C_a}{C} \quad (2)$$

$$\frac{C_a}{C} = \frac{\left(\frac{H_a}{H} \cdot \frac{H}{C}\right)}{\frac{H_a}{C_a}} \quad (3)$$

$$\frac{H_a}{H} = \frac{A_{3000\sim 2800}}{(A_{900\sim 700} + A_{3000\sim 2800})} \quad (4)$$

where C_a/C is the proportion of fat carbon in the carbon element, H/C is the ratio of hydrogen to carbon and H_a/C_a is the proportion of hydrogen and carbon atoms in fat clusters (generally about 1.8. H_a/H is the percentage of aliphatic hydrogen in hydrogen atoms).

3.3.3. Aromaticity I

Aromaticity is an important parameter used to determine the aromaticity of substances. Aromaticity is defined by the ratio of aromaticity to aliphatic carbon.

$$I_1 = \frac{A_{3100\sim 3000}}{A_{3000\sim 2800}} \quad (5)$$

$$I_2 = \frac{A_{900\sim 700}}{A_{3000\sim 2800}} \quad (6)$$

where $3100\text{--}3000\text{ cm}^{-1}$ is mainly aromatic C-H stretching vibration, $3000\text{--}2800\text{ cm}^{-1}$ is aromatic CH_x stretching vibration and $900\text{--}700\text{ cm}^{-1}$ absorption position of aromatic structure.

3.3.4. Degree of Aromatic Ring Condensation *DOC*

The degree of aromatic ring condensation can also be used to judge the degree of coal rank. The higher the coal metamorphism, the more the internal carbon content, and the more condensed aromatic substances.

$$DOC = \frac{A_{700\sim 900}}{A_{1490\sim 1600}} \quad (7)$$

where the ratio of $900\text{--}700\text{ cm}^{-1}$ to $1490\text{--}1600\text{ cm}^{-1}$ indicates the degree of aromatic ring condensation.

3.3.5. $A_{\text{CH}_2}/A_{\text{CH}_3}$

$A_{\text{CH}_2}/A_{\text{CH}_3}$ is the fat structure parameter [48]. CH_2 mainly has a chain, ring and aromatic side hydrocarbon straight chain, while CH_3 mainly has a chain, ring side chain and aromatic side hydrocarbon branched chain.

$$\frac{A_{\text{CH}_2}}{A_{\text{CH}_3}} = \frac{A_{2920}}{A_{2950}} \quad (8)$$

3.3.6. Maturity *Csd*

The maturity of coal is indicated by the large change in the carbon–oxygen double bond relative to the carbon–carbon double bond.

$$Csd = \frac{A_{1800\sim 1650}}{A_{1800\sim 1650} + A_{1600}} \quad (9)$$

3.4. Summary of Structural Parameters of Infrared Spectroscopy

The outburst coal and primary coal f_{Ha} , f_{C} , I_1 , I_2 , *DOC*, $A_{\text{CH}_2}/A_{\text{CH}_3}$ and *Csd* are calculated by Equations (1)–(9). The calculation results are shown in Table 3.

Table 3. Structure parameters summary table.

Component	f_{Ha}	f_{C}	I_1	I_2	<i>DOC</i>	$A_{\text{CH}_2}/A_{\text{CH}_3}$	<i>Csd</i>
Coal Samples							
outburst coal	0.271	0.986	0.477	0.373	1.560	0.850	0.969
primary coal	0.229	0.984	0.454	0.298	1.010	0.916	0.976

The analysis shows that the aromatic hydrogen rate (f_{Ha}) and aromatic carbon rate (f_{C}) of outburst coal are higher than those of primary coal, indicating that the hydrogen and carbon elements in aromatic functional groups are higher. The aromaticity I_1 and I_2 of outburst coal were higher than those of raw coal, indicating that the aliphatic functional group of outburst coal was higher than that of the aromatic structural functional group. The aromatic ring polycondensation degree (*DOC*) of the outburst coal is higher than that of the primary coal and the hydrogen content is also higher than that of the primary coal, while $A_{\text{CH}_2}/A_{\text{CH}_3}$ and maturity (*Csd*) are slightly less than native coal, indicating that native coal has more straight chains than side chains, while aliphatic hydrocarbons are mostly short chains and have high branched degree. The results are consistent with previous studies, i.e., coal degree is inversely proportional to $A_{\text{CH}_2}/A_{\text{CH}_3}$.

3.5. X-ray Diffraction (XRD) Analysis of Coal Samples

3.5.1. XRD Peak Fitting

In order to analyze the microstructure of outburst coal, the XRD patterns of coal samples were fitted by peak separation, as shown in Figure 11. The original spectrum was divided into 002 peaks, γ peaks and 100 peaks by Gaussian [41] formula. The fitting formula is:

$$y = y_0 + \frac{A}{w \cdot \sqrt{\frac{\pi}{2}}} \cdot e^{-2\left(\frac{x-x_c}{w}\right)^2} \quad (10)$$

where y_0 is the baseline position, w is the diffraction peak width, A is the diffraction pattern area and x_c is the 2θ angle of the diffraction center.

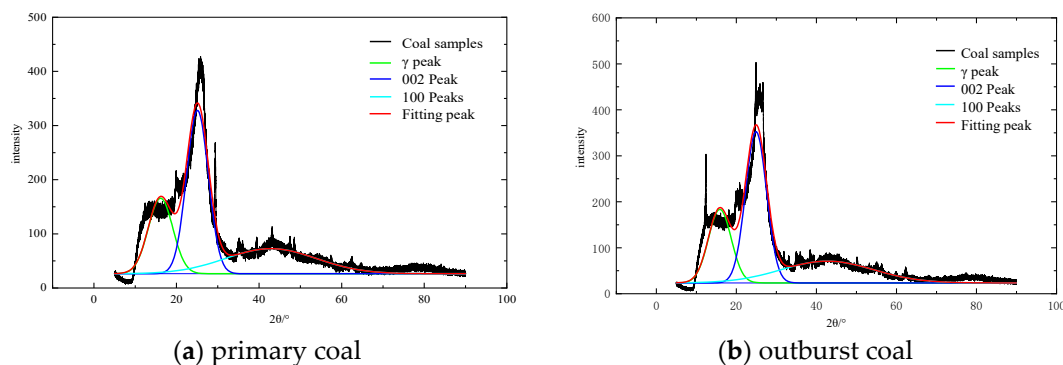


Figure 11. Peak separation fitting results of coal samples.

It can be found from Figure 11 and Table 4 that the 2θ angle range of 002 diffraction peak is 24.92° – 25.08° , with high intensity and good symmetry. Moreover, the 2θ angle range of 100 diffraction peaks is 42.73° – 42.85° and the diffraction peaks are wide and low, indicating that the degree of aromatic ring condensation in coal is not high. For the γ band, it can be clearly seen from the graph that its area is large, reflecting the rich branched chain structure of aliphatic hydrocarbons and aliphatic hydrocarbons in coal.

Table 4. Diffraction peak fitting of the main 2θ parameters.

Coal Samples	Diffraction Peak		
	002 Peak	100 Peak	γ Peak
outburst coal	24.92	42.73	15.87
primary coal	25.08	42.85	16.15

3.5.2. Structure Analysis of Aromatic Microcrystals

The layer spacing of d_{002} and d_{100} , the average stacking height of L_c and the ductility of L_a of the aromatic layer can be calculated from the diffraction angle and the half-peak width [49].

$$d_{002/100} = \frac{\lambda}{2 \sin \theta_{002/100}} \quad (11)$$

$$L_c = \frac{K_1 \lambda}{\beta_{002} \cos \theta_{002}} \quad (12)$$

$$L_a = \frac{K_2 \lambda}{\beta_{100} \cos \theta_{100}} \quad (13)$$

$$M_c = \frac{L_c}{d_{002}} \quad (14)$$

where λ is the wavelength of X-ray, and 0.15405 nm is used for the experiment with copper target irradiation; $\theta_{002/100}$ is the Bragg angle of 002 diffraction peak and 100 diffraction

peak, respectively; β_{002} and β_{100} are the half-peak widths of 002 diffraction peak and 100 diffraction peak, respectively; K_1 and K_2 are Debye-Scherrer constants, with K_1 as 0.89, K_2 as 1.84 and M_c as the number of effective stacked aromatic slices.

In general, the interlayer spacing of the coal aromatic layer is between cellulose ($d_{002} = 3.975 \times 10^{-1}$ nm) and graphite ($d_{002} = 3.354 \times 10^{-1}$ nm). Therefore, the coalification degree P is used to determine the percentage of condensed aromatic ring, and the relative content of aromatic layer and aliphatic layer structure is obtained. The calculation formula is as follows:

$$P = \frac{3.975 - d_{002}}{3.975 - 3.354} \times 100\% \quad (15)$$

The calculation results are shown in Table 5. It can be found from the table that d_{002} of primary coal is 3.548, indicating that its coalification degree is high. The number of effective stacking aromatic slices of primary coal is about 4, and the coalification degree is 68.83%, indicating that the coal sample has a high degree of coalification, with fewer side chains and functional groups, and the internal arrangement of molecules is orderly and stable, and the condensation degree of aromatic nucleus is high. Combined with the data of d_{002} and d_{100} , the number of aromatic flakes in outburst coal is lower than primary coal, which suggests that the prominent heating effect increases the degree of aromatization, increases the d_{100} and d_{002} values and, finally, changes the dense ring structure in coal. Through the coal degree index P , it can be seen that the primary coal is slightly higher than the outburst coal. Combined with the analysis of d_{002} and d_{100} as basically unchanged, this shows that the content of side chain in the primary coal is lower than that of the outburst coal, resulting in the increase of the relative number of aromatic rings, which is finally reflected in the increase of P .

Table 5. XRD microstructure parameters of coal samples.

Coal Samples	d_{002}	d_{100}	L_c	L_a	M_c	P
outburst coal	3.570	2.114	13.016	3.089	3.646	65.22%
primary coal	3.548	2.109	12.951	3.240	3.651	68.83%

4. Conclusions

- (1) The proximate analysis results show that the volatile matter and moisture content of outburst coal are higher than those of primary coal, but that the ash content is lower than that of primary coal. The ultimate analysis shows that the proportions of N and S in outburst coal and primary coal are small.
- (2) The aromatic structure absorption band analysis showed that the trisubstituted benzene ring and the disubstituted benzene ring in the primary coal were higher than that in outburst coal, and that the tetrasubstituted benzene ring and the pentasubstituted benzene ring in outburst coal were higher than that in primary coal. This may be due to the substitution reaction of fat chain cyclization and the orientation group of the aromatic ring. The absorption band of fat structure indicates that hydrogen volatilization or fat chain rupture is caused by thermal effect in the outburst process. Moreover, the hydroxyl absorption band shows that the internal structure of the molecule is tighter, which increases the probability of self-association hydroxyl synthesis.
- (3) By analyzing and calculating the structural parameters of infrared spectroscopy, it is concluded that the aromatic hydrogen rate, aromatic carbon rate and I_1 and I_2 of outburst coal are higher than those of primary coal. The A_{CH_2}/A_{CH_3} raw coal is relatively low, and the maturity is slightly higher than that of the outburst coal, indicating that the raw coal has more straight chains than side chains and that the aliphatic hydrocarbons are mostly short chains and have high branched degree.
- (4) Through the analysis and calculation of XRD microcrystalline structure parameters, the number of aromatic flakes in outburst coal is lower than in primary coal, which suggests that the prominent heating effect increases the degree of aromatization,

increases the d_{100} and d_{002} values and, finally, changes the dense ring structure in coal. Moreover, from the coal degree index P , it can be seen that the primary coal has a smaller increase than the outburst coal.

Author Contributions: Conceptualization: A.J., S.T.; Methodology: H.L.; Formal analysis and investigation: A.J., H.L.; Writing—original draft preparation: A.J.; Writing—review and editing: S.T.; Funding acquisition: S.T. All authors have read and agreed to the published version of the manuscript.

Funding: This work was supported by the National Natural Science Foundation of China under Grant number 52104079 and the Science & Technology Foundation of Guizhou Province under Grant number [2020]4Y050.

Informed Consent Statement: Informed consent was obtained from all subjects involved in the study.

Data Availability Statement: All data, models, and code generated or used during the study appear in the submitted article.

Acknowledgments: The authors appreciate the support from above funders.

Conflicts of Interest: The authors declare that they have no competing financial interests.

References

1. Li, X.-L.; Cao, Z.-Y.; Xu, Y.-L. Characteristics and trends of coal mine safety development. *Energy Sour. Part A* **2020**, *12*, 1–14. [[CrossRef](#)]
2. Tang, X.-G. Occurrence Regularity of Coal Resources in Guizhou Province. *Coal Geol. Explor.* **2012**, *40*, 1–5.
3. Zhao, Z.-H.; Kuang, S.-D. Thoughts on Development of Coal Resources in Guizhou. *China Min. Mag.* **2006**, *3*, 17–20, 28.
4. Jia, H.-F.; An, F.-H. Experimental Study on Influence of Gas Occurrence State on Strength of Granular Coal. *Saf. Coal Mines* **2020**, *51*, 29–33.
5. Wang, W.; Wei, Y.-Z.; Jia, T.-R.; Yan, J.-G. Deformation Characteristics and Gas Occurrence Regularity of Coal Measures in North. *Coal Geol. Explor.* **2021**, *49*, 121–130.
6. Kong, S.-S.; Yang, Y.; Jia, Y.; Song, Y.-Q.; Sun, T.-L.; Kang, R.-P. Study on Gas Occurrence Characteristics and Influence of Key Geological Factors in Coal Seam. *Coal Sci. Technol.* **2019**, *47*, 53–58.
7. Jia, T.-R.; Wang, W.; Yan, J.-G.; Tang, C.-A. Control law and zoning of gas occurrence structure in Guizhou coal mines. *Earth Sci. Front.* **2014**, *21*, 281–288.
8. Zhang, P.-X.; Long, Z.-G. Study on Gas Occurrence Law of Coal Mines in Guizhou Province. *J. Saf. Sci. Technol.* **2013**, *9*, 34–38.
9. Lin, H.-Y.; Tian, S.-X.; Jiao, A.-J.; Ma, R.-S.; Xu, S.-Q. Pore Characteristics and Fractal of Tectonic Coal and Primary Coal in Northern Guizhou. *Sci. Technol. Eng.* **2021**, *21*, 14451–14458.
10. Yan, M.; Yue, M.; Lin, H.-F.; Yan, D.-G.; Wei, J.-N.; Qin, X.-Y.; Zhang, J. Experimental Study on Effect of Functional Groups on Wettability of Medium and Low Rank Coal. *Coal Sci. Technol.* **2022**; *unpublished*.
11. He, X.; Wang, W.-F.; Zhang, X.-X.; Yang, Y.-T.; Sun, H. Distribution characteristics and differences of oxygen functional groups in macerals of low rank coal. *J. China Coal Soc.* **2021**, *46*, 2804–2812.
12. Chen, Y.-Y.; Mastalerz, M.; Schimmelmann, A. Characterization of chemical functional groups in macerals across different coal ranks via micro-FTIR spectroscopy. *Int. J. Coal Geol.* **2012**, *104*, 22–33. [[CrossRef](#)]
13. Guo, Y.; Bustin, R.-M. Micro-FTIR Spectroscopy of Liptinite Macerals in Coal. *Int. J. Coal Geol.* **1998**, *36*, 259–275. [[CrossRef](#)]
14. Karayigita, A.-I.; Bircan, C.; Mastalerz, M.; Oskay, R.-G.; Querol, X.; Lieberman, N.-R.; Turkmen, I. Coal characteristics, elemental composition and modes of occurrence of some elements in the İsaalan coal (Balıkesir, NW Turkey). *Int. J. Coal Geol.* **2017**, *172*, 43–59. [[CrossRef](#)]
15. Mastalerz, M.; Bustin, R.-M. Electron microprobe and micro-FTIR analyses applied to maceral chemistry. *Int. J. Coal Geol.* **1993**, *24*, 333–345. [[CrossRef](#)]
16. He, X.; Zhang, X.-X.; Jiao, Y.; Zhu, J.-S.; Chen, X.-W.; Li, C.Y.; Li, H.-S. Complementary analyses of infrared transmission and diffuse reflection spectra of macerals in low-rank coal and application in triboelectrostatic enrichment of active maceral. *Fuel* **2017**, *192*, 93–101. [[CrossRef](#)]
17. Arif, M.; Jones, F.; Barifcani, A.; Iglauer, S. Influence of surface chemistry on interfacial properties of low to high rank coal seams. *Fuel* **2017**, *194*, 211–221. [[CrossRef](#)]
18. Xin, H.-H.; Wang, D.-M.; Dou, G.-L.; Qi, X.-Y.; Xu, T.; Qi, G.-S. The infrared characterization and mechanism of oxygen adsorption in coal. *Spectrosc. Lett.* **2014**, *47*, 664–675. [[CrossRef](#)]
19. Jia, T.-G.; Li, C.; Qu, G.-N.; Li, W.; Yao, H.-F.; Liu, T.-F. FTIR characterization of chemical structure characteristics of coal samples with different metamorphic degrees. *Spectrosc. Spectr. Anal.* **2021**, *41*, 3363–3369.
20. Liang, C.-H.; Liang, W.-Q.; Li, W. Study on Functional Groups of Different Rank Coals Based on Fourier Transform Infrared Spectroscopy. *J. China Coal Soc.* **2020**, *48*, 182–186.

21. Wang, C.; Zhao, Y.-B.; Wang, Z.-W.; Lu, Z.-L. Improved method for characterizing coal metamorphic degree by XRD. *China Coal Geol. Explor.* **2019**, *47*, 39–44.
22. Li, X.; Liu, Z.; Qian, J. Analysis on the Changes of Functional Groups after Coal Dust Explosion at Different Concentrations Based on FTIR and XRD. *Combust. Sci. Technol.* **2020**, *193*, 2482–2504. [[CrossRef](#)]
23. Presswood, S.-M.; Rimmer, S.-M.; Anderson, K.-B.; Filiberto, J. Geochemical and petrographic alteration of rapidly heated coals from the Herrin (No. 6) Coal Seam, Illinois Basin. *Int. J. Coal Geol.* **2016**, *165*, 243–256. [[CrossRef](#)]
24. Yan, J.; Lei, Z.; Li, Z.; Wang, Z.; Ren, S.; Kang, S.; Wang, X.; Shui, H. Molecular structure characterization of low-medium rank coals via XRD, solid state ¹³CNMR and FTIR spectroscopy. *Fuel* **2020**, *268*, 117038. [[CrossRef](#)]
25. Kwiecinska, B.; Pusz, S.; Valentine, B.-J. Application of electron microscopy TEM and SEM for analysis of coals, organic-rich shales and carbonaceous matter. *Int. J. Coal Geol.* **2019**, *211*, 103203. [[CrossRef](#)]
26. Liu, M.; Bai, J.; Jianglong, Y.-U.; Kong, L.; Bai, Z.; Li, H.; He, C.; Ge, Z.; Cao, X.-I.; Li, W. Correlation between char gasification characteristics at different stages and microstructure of char by combining X-ray diffraction and Raman spectroscopy. *Energy Fuels* **2020**, *34*, 4162–4172. [[CrossRef](#)]
27. Li, X.; Yiwen, J.-U.; Hou, Q.; Li, Z. FTIR and Raman spectral research on metamorphism and deformation of coal. *J. Geol. Res.* **2012**, *2012*, 590857. [[CrossRef](#)]
28. Li, W.; Zhu, Y.-M.; Chen, S.-B.; Si, Q.-H. Coupling mechanism of hydrocarbon generation and structural evolution in low coal grade coal. *Spectrosc. Spectr. Anal.* **2013**, *33*, 1052–1056.
29. Li, W.; Zhu, Y.-M.; Wang, G.; Jiang, B. Characterization of coalification jumps during high rank coal chemical structure evolution. *Fuel* **2016**, *185*, 298–304. [[CrossRef](#)]
30. He, X.-Q.; Liu, X.-F.; Nie, B.-S.; Song, D.-Z. FTIR and Raman spectroscopy characterization of functional groups in various rank coals. *Fuel* **2017**, *206*, 555–563. [[CrossRef](#)]
31. Ibarra, J.; Muñoz, E.; Moliner, R. FTIR study of the evolution of coal structure during the coalification process. *Org. Geochem.* **1996**, *24*, 725–735. [[CrossRef](#)]
32. Sobkowiak, M.; Reisser, E.; Given, P. Determination of aromatic and aliphatic CH groups in coal by FT-IR:1. Studies of coal extracts. *Fuel* **1984**, *9*, 1245. [[CrossRef](#)]
33. Dela Rosa, L.; Pruski, M.; Lang, D. Characterization of the Argonne premium coals by using hydrogen-1 and carbon-13 NMR and FT-IR spectroscopies. *Energy Fuels* **1992**, *6*, 460. [[CrossRef](#)]
34. Alemany, L.-B.; Grant, D.-M.; Pugmire, R.-J. Solid state magnetic resonance spectra of Illinois No. 6 coal and some reductive alkylation products. *Fuel* **1984**, *63*, 513–521. [[CrossRef](#)]
35. Painter, P.-C.; Sobkowiak, M.; Youtcheff, J. FT-IR Study of hydrogen-bonding in coal. *Fuel* **1987**, *66*, 973–978. [[CrossRef](#)]
36. Orrego-Ruiz, J.-A.; Cabanzo, R.; Mejía-Ospino, E. Study of Colombian coals using photoacoustic Fourier transform infrared spectroscopy. *Int. J. Coal Geol.* **2011**, *85*, 307–310. [[CrossRef](#)]
37. Cao, X.; Chappell, M.-A.; Schimmelmann, A.; Mastalerz, M.; Li, Y.; Hu, W. Chemical structure changes in kerogen from bituminous coal in response to dike intrusions as investigated by advanced solid-state ¹³C NMR spectroscopy. *Int. J. Coal Geol.* **2013**, *108*, 53–64. [[CrossRef](#)]
38. Gupta, R. Advanced coal characterization: A review. *Energy Fuels* **2017**, *21*, 451–460. [[CrossRef](#)]
39. Machado, A.D.S.; Mexias, A.S.; Vilela, A.C.F.; Osorio, E. Study of coal, char and coke fines structures and their proportions in the off-gas blast furnace samples by X-ray diffraction. *Fuel* **2013**, *114*, 224–228. [[CrossRef](#)]
40. Song, D.; Yang, C.; Zhang, X.; Su, X.-B.; Zhang, X. Structure of the organic crystallite unit in coal as determined by X-ray diffraction. *Min. Sci. Technol.* **2011**, *21*, 667–671. [[CrossRef](#)]
41. Cartz, L.; Hirsch, P.-B. A contribution to the structure of coals from X-ray diffraction studies. *Philos. Trans. R. Soc. Lond.* **1960**, *252*, 557–602.
42. Li, M.; Zeng, F.; Chang, H.; Bingshe, X.; Wang, W. Aggregate structure evolution of low-rank coals during pyrolysis by in-situ X-ray diffraction. *Int. J. Coal Geol.* **2013**, *116–117*, 262–269. [[CrossRef](#)]
43. Saikia, B.-K.; Boruah, R.-K.; Gogoi, P.-K. XRD and FT-IR investigations of sub-bituminous Assam coals. *Bull. Mater. Sci.* **2007**, *30*, 421–426. [[CrossRef](#)]
44. Wu, D.; Liu, G.; Sun, R.; Xiang, F. Investigation of structural characteristics of thermally metamorphosed coal by FTIR spectroscopy and X-ray diffraction. *Energy Fuels* **2013**, *27*, 23–30.
45. Jiang, J.-Y.; Yang, W.-P.; Cheng, Y.-P.; Liu, Z.-D.; Zhang, Q.; Zhao, K. Molecular structure characterization of middle-high rank coal via XRD, Raman and FTIR spectroscopy: Implications for coalification. *Fuel* **2019**, *239*, 559–572. [[CrossRef](#)]
46. Boral, P.; Varma, A.-K.; Maity, S. X-ray diffraction studies of some structurally modified Indian coals and their correlation with petrographic parameters. *Curr. Sci.* **2015**, *108*, 384–394.
47. Yan, J.; Bai, Z.; Zhao, H.; Bai, J.; Li, W. Inappropriateness of the standard method in sulfur form analysis of char from coal pyrolysis. *Energy Fuels* **2012**, *26*, 37–42. [[CrossRef](#)]
48. Fu, Y.; Liu, X.-F.; Ge, B.-Q.; Liu, Z.-H. Role of chemical structures in coalbed methane adsorption for anthracites and bituminous coals. *Adsorption* **2017**, *23*, 711–721. [[CrossRef](#)]
49. Matthews, M.-J.; Pimenta, M.-A.; Dresselhaus, G.; Dresselhaus, M.-S. Origin of dispersive effects of the Raman D band in carbon materials. *Phys. Rev. B* **1999**, *59*, 6585–6588. [[CrossRef](#)]